Palaeoenvironmental change and glacier fluctuations in the high Tian Shan Mountains during the last millennium based on sediments from Lake Ala Kol, Kyrgyzstan

Marine Rousseau, François Demory, Cécile Miramont, Elodie Brisset, Frédéric Guiter, Pierre Sabatier, Philippe Sorrel

Palaeoenvironmental change and glacier fluctuations in the high Tian Shan Mountains during the last millennium based on sediments from Lake Ala Kol, Kyrgyzstan

Marine Rousseau[a,*], François Demory[b], Cécile Miramont[c,d], Elodie Brisset[c,d,e], Frédéric Guiter[c,d], Pierre Sabatier[f], Philippe Sorrel[g]

[a] UMR CNRS 6249 Chrono-Environnement, Université Franche-Comté, 16 route de Gray, 25030 Besançon, France
[b] Aix Marseille Univ, CNRS, IRD, INRAE, Coll France, CEREGE, Aix-en-Provence, France
[c] Aix Marseille Univ, CNRS, Université d'Avignon, IRD, UMR 7263 IMBE, Europôle Méditerranéen de l'Arbois, BP 80, 13545 Aix-en-Provence Cedex 4, France
[d] ECCOREV Research Federation, Europôle Méditerranéen de l'Arbois, BP 80, 13545 Cedex 4 Aix-en-Provence, France
[e] Institut Català de Paleoecología Humana i Evolució Social (IPHES), Àrea de Prehistòria, Universitat Rovira i Virgili, 43007 Tarragona, Spain
[f] Univ. Grenoble Alpes, Univ. Savoie Mont Blanc, CNRS, EDYTEM, Chambéry, France
[g] Univ Lyon, Univ Lyon 1, ENSL, CNRS, LGL-TPE, F-69622, Villeurbanne, France

ARTICLE INFO

Keywords:
Paleohydrology
Paleomagnetism
Rock magnetism
Proglacial lake
Central Asia

ABSTRACT

A suite of limnological proxies measured in clastic sediments of the glacier-fed Lake Ala Kol (NE Kyrgyzstan) document palaeoenvironmental change and glacier fluctuations in the central Tian Shan over the last millennium. Rock magnetic and geochemical data provide supporting evidence for three glacier expansion episodes occurring in 1200–1400 CE, 1500–1850 CE and 1900–1950 CE and glacier retreat periods during 1000–1200 CE and the intervening periods. The maximal glacier extent, as inferred from high κ_{LF}, Si/inc + coh, Ca/inc + coh and low ARM_{30}/ARM, is recorded between 1500 and 1850 CE and corresponds to cold and wet conditions during the Little Ice Age in the high central Tian Shan. Periods of glacier waxing and waning recorded at Lake Ala Kol present a close correspondence to ice accumulation rate in the northern Tibetan Plateau, suggesting that precipitation changes are the main driver of glacier fluctuations in central Tian Shan during the last millennium, although temperature may have exerted a more complex influence on centennial timescales.

1. Introduction

Glaciers in the Tian Shan Mountains, as with many glaciers worldwide, have been thinning since the end of the Little Ice Age (LIA) in the mid-nineteenth century, a propensity that has strengthened since the 1960s with significant glacier reduction in the Kyrgyz region (Bolch, 2007; Kutuzov and Shahgedanova (2009); Niederer et al., 2007; Narama et al., 2006, 2009; Sorg et al., 2012). On average, Tian Shan glaciers have retreated by 989 ± 540 m since the coldest and wettest years of the LIA, while their front elevation rose by 151 ± 105 m (Solomina et al., 2004). Discerning the timing of temperature and precipitation variations in Central Asia is necessary for a better understanding of global climate change (IPCC, 2013). In this regard, it has been shown that the LIA glaciers in the warm and humid northwestern periphery of the Tian Shan were significantly more extensive than the glaciers in more central areas (Savoskul and Solomina, 1996). This contrast seems linked to regional differences in moisture between peripheral and inner areas of the mountain massif (Savoskul and Solomina, 1996; Savoskul, 1997). Nowadays, the most dramatic shrinkage occurs in the outer ranges of the Tian Shan (Narama et al., 2009). As few records of glacier fluctuations are available to date for the Tian Shan, fundamental questions remain open regarding the relative contribution of precipitation and temperature to glacier mass-balance, especially at the centennial to millennial scale. In particular, high-resolution palaeolimnological records from glacier-fed lakes are lacking in the Tian Shan. Proglacial lakes can provide continuous records of glacier fluctuations since glacially eroded particles are transported by meltwater streams and deposited on lake bottoms (Bakke et al., 2010; Fouinat et al., 2017; Liu et al., 2014; Matthews et al., 2000; Nesje et al., 2001; Røthe et al., 2018; van der Bilt et al., 2015; Wittmeier et al., 2015).

Here, we aim to improve our understanding of glacier fluctuations and related climatic change in the Tian Shan over the last millennium based on the first short-core sequence retrieved from Lake Ala Kol, a

* Corresponding author.
E-mail address: marine.rousseau@univ-fcomte.fr (M. Rousseau).

https://doi.org/10.1016/j.palaeo.2020.109987
Received 30 December 2019; Received in revised form 18 August 2020; Accepted 18 August 2020

high-altitude glacier-fed lake from NE Kyrgyzstan. Our objectives are threefold: (1) to build-up a continuous and high-resolution record of glacial variations in central Tian Shan based on glaciolacustrine sediments from Lake Ala Kol, (2) to compare those results with other available records from the Pamir and Kunlun Mountains (northern Tibetan Plateau) for the last millennium and, (3) to compare our findings with proxy reconstructions of regional precipitation and temperature in order to decipher the effects of both variables on glacial variability at centennial to sub-millennial time scales.

2. Environmental and climatic setting

Lake Ala Kol (42°19′1.80″N; 78°32′4.79″E) is located at 3560 m above sea level (m.a.s.l) in the central Tian Shan Mountains, 20 km southeast of Karakol in NE Kyrgyzstan (Fig. 1). It is a rock-damned proglacial lake covering an area of ~1.6 km^2 (2.3-km long, 0.7-km wide). The lake is elongated and 70 m deep. The catchment area covers ~10 km^2 and includes several peaks that culminate at up to 4200 m.a.s.l. Its bedrock mainly consists of granites, granodiorites and leucogranites. The drainage area includes a granite-granodiorite complex of Late Ordovician-early Silurian age (resources map of Kyrgyz Republic; Nikonorov et al., 2000). Due to geomorphological settings, scree slopes (almost deprived of vegetation) around the lake are very steep and one avalanche corridor is present at the westernmost part of the lake, close to the outflow (Fig. 1). The occurrence of snow accumulation at the corridor terminus was observed on the frozen lake in April 2019. Vegetation in the catchment is rare and only consists of a few species of herb (*Poa litwinoviana, Avenastrum schellianum*) and moss (*Tortula moralis, T. fragilis, T. rualis*). This accounts for the absence of terrestrial macrorests (e.g., plant remains) in the lake sediments that could be used for ^{14}C dating. The surface of Lake Ala Kol is frozen nine months out of the year and snow covers most of its watershed. In

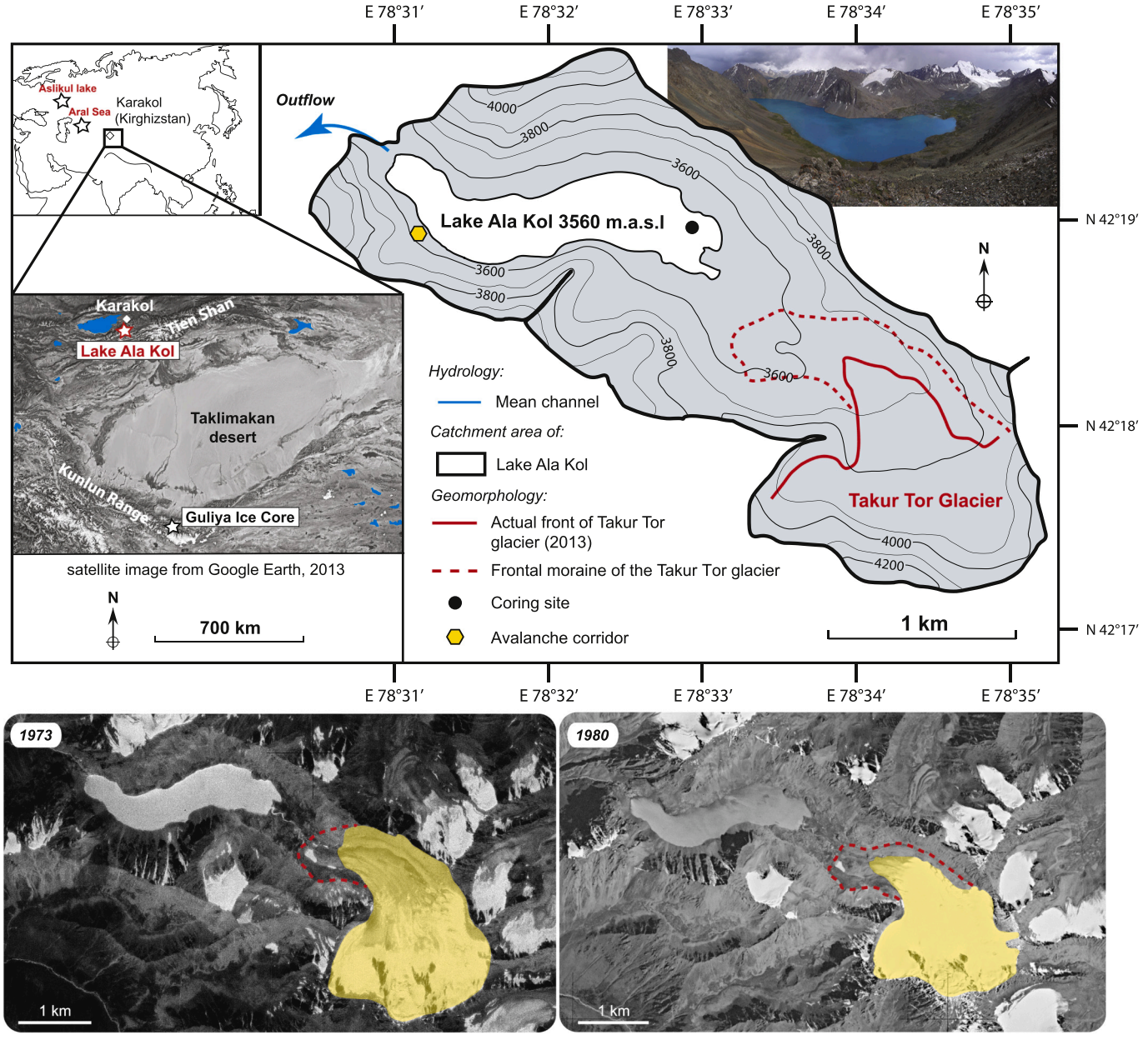

Fig. 1. Location and geomorphological setting of Lake Ala Kol in central Tian Shan (Kyrgyzstan), and the Takur Tor glacier in the lake catchment. Satellite images from 1973 CE (31.07.1973) and 1980 CE (21.08.1980) have been extracted from https://earthexplorer.usgs.gov/.
Yellow shading on satellite images corresponds to the past extent of the Takur Tor glacier in 1973 CE and 1980 CE, while the red dashed line refers to the frontal (LIA?) moraine of the glacier. (For interpretation of the references to colour in this figure legend, the reader is referred to the web version of this article.)

summer, the Takur Tor glacier experiences surface melting, which supplies ample snowmelt runoff to the lake. The Takur Tor glacier is a small mountain glacier (cirque or niche-type) according to the primary classification of the World Glacier Inventory (http://nsidc.org/data/glacier_inventory), with a single accumulation area, and no visible debris on the glacier surface. The glacier is perched on a steep mountain side facing north and is mostly nourished by snow. The snow line elevation is 3800 m.a.s.l. upstream from the lake. Terminal moraines exhibit a marked retreat since 1973 and 1980 CE (Fig. 1). Glacier (ice) accumulation occurs mainly in spring/summer, highlighting that the seasons of highest accumulation and ablation are close or even coeval. It is therefore characteristic of the "summer-accumulation glacier type" as reported from other glaciers in Kyrgyzstan (Narama et al., 2009). Lake Ala Kol is a purely natural lake undisturbed by human activities in the watershed (no pastoral activities).

Modern climate conditions correspond to a steppe-type (dry and cold) climate, classified as a BSk climate according to the Köppen-Geiger classification (Peel et al., 2007). Seasonal and annual precipitation varies significantly throughout the Tian Shan Mountains (Narama et al., 2009). Higher annual precipitation characterizes the Ili-Kungöy region (including the area of the Lake Ala Kol area) in the outer mountain ranges of central Tian Shan, compared to the more interior areas (Narama et al., 2009). This spatial variability is due to the blocking of moisture carried by the Westerlies. In the Ili-Kungöy region of Lake Aka Kol, mean annual precipitation ranges between 80 and 300 mm, and the warmest and coldest months are characterized by temperatures averaging 14 and − 15 °C, respectively (Tian Shan station, 3614 m.a.s.l.). Interactions between the Westerlies and the Siberian High Pressure system control seasonal climate conditions over the Tian Shan to a great extent (Aizen et al., 1997, 2001; Böhner, 2006).

3. Material and methods

3.1. Lake coring

The 60-cm long sediment core Ala-04 was collected from Lake Ala Kol (N42°19′03.7″, E78°32′59.5″, 3560 m.a.s.l) in July 2014, in the frame of a pilot investigation (Fig. 1). To our knowledge, this is the first such core ever retrieved from Lake Ala Kol. The sediment core was recovered from a boat using a non-magnetic gravity corer (UWITEC device). Such a coring approach prevents core twisting. The core Ala-04 was retrieved at about 80 m from the shore, in a water depth of ca. 10 m (Fig. 1). A few specimens of amphipods were found in the sediment-water interface; however none were discovered within the sediments despite wet sieving with 63 μm mesh and microscope analysis. Core Ala-04 was obtained in a relatively proximal position to the main tributary (Fig. 1). However, due to the absence of avalanche corridors identified in the vicinity of our coring site, the likelihood of debris flows (transporting gravel from the steep slopes) within the sediments of core Ala-04 is very low. Lithological description and photographs were performed directly after core opening on split core-half surfaces.

3.2. Rock magnetism and sedimentology

Rock magnetic and palaeomagnetic analyses were conducted at the CEREGE institute (France). The uppermost sediment was not water-saturated and was thus suitable for subsampling. Core Ala-04 was continuously subsampled using 2 cm^3 plastic cubes pushed into the split surface at intervals of 1.5 cm. Rock magnetic analyses were conducted in this study to (1) evaluate the quality (e.g., magnetic mineralogy, magnetic grain size) of the magnetic components and (2), provide a set of proxies to track glaciogenic (clastic) sediment input to Lake Ala Kol. Low field magnetic susceptibility (κ_{LF}) is generally used as a proxy for tracking terrestrial inputs in sediments and κ_{LF} is linked with magnetic mineral concentration. κ_{lF} was measured using a AGICO MFK1 Kappabridge. κ_{LF} is mainly controlled by ferromagnetic minerals (e.g., magnetite), but can also be influenced to a minor extent by diamagnetic (i.e., carbonates) or paramagnetic material (i.e., clays).

All remanent magnetization analyses were conducted using a fully automated superconducting rock magnetometer (2G Enterprises DC SQUID 760 SRM). Natural Remanent Magnetization (NRM) was stepwise demagnetized using an alternating field (AF) up to 100 mT with steps of 5 mT. NRM analyses were conducted on 39 samples from core Ala-04. For each sample we determined a Characteristic Remanent Magnetization (ChRM), which corresponds to the stable magnetization representing the orientation of the Earth's Magnetic field at the location and time (or shortly after) of sedimentary deposition. Inclination and declination vary at the secular scale (Thouveny et al., 2004), thus defining the paleo-secular variations (PSV) of the geomagnetic field. Values of ChRM were obtained through a Principal Component Analysis (PCA) of the demagnetization patterns of the NRM (Kirschvink, 1980) on the stable component. For ChRM determinations, we used the software PuffinPlot (Lurcock and Wilson, 2012). A Maximum Angular Deviation (MAD) was calculated for each sample in order to evaluate the deviation of each demagnetization point from the linear regression, since only MAD values $< 5^{\circ}$ have been shown to be reliable (Stoner and St-Onge, 2007). Relative Paleointensity (RPI) was estimated, but the results were not conclusive; the coarse size of the ferromagnetic grains made the ratio of NRM with any concentration parameter (κ_{LF}, ARM, IRM) impossible to interpret in terms of relative geomagnetic field paleointensity (Spassov and Valet, 2012). In addition, the evaluation of post-depositional remanent magnetization (usually referred as the

Table 1
Age anchor points, sedimentation rates and lock-in-depth data for core Ala-04. Age anchor points are based on the correlation of PSV data (inclination and declination) with (1) the Aral Sea and Lake Aslikul records and (2) the GUFM1, ARCH3k.1 and CALSK3k.4 models. Note that D1 is not precisely identified in core Ala-04 and is therefore excluded from the age model.

Inclination					Sed rates ($cm.yr^{-1}$)	Lock-in-depth (cm)	Lock-in-depth (yr)
Depth (cm)	Gumf1 (Jackson et al., 2000)	Aral Sea/Lake Aslikul (Nourgaliev et al., 2003)	CALS3K (Korte et al., 2011)	ARCH3K.1 (Korte et al., 2009)			
	Years AD	Years AD	Years AD	Years AD			
14 (i1)	1750 ± 50	1750 ± 50	1725 ± 75?	1650 ± 50	0,050	1,4	28,5
23 (I2)	1550 ± 50	1550 ± 50	1500 ± 50	1600 ± 50?	0,044	3,2	74,3
37 (I3)	n/a	1250 ± 50	1300 ± 50	1400 ± 50?	0,050	5,2	103,0
48 (I4)	n/a	1150 ± 50	1150 ± 50	1225 ± 50?	0,080	3,5	44,1
Declination							
n/a (D1)	1900 ± 50	1850 ± 50	1900 ± 50	1900 ± 50			
23 (d2)	1550 ± 50	1550 ± 50	1650 ± 50	1650 ± 50	0,044	3,2	74,3
32 (D3)	n/a	1350 ± 50	n/a	1150 ± 50	0,047	5,3	106,0

paleomagnetic lock-in-depth) was undertaken in core Ala-04 (Table 1). The paleomagnetic lock-in-depth corresponds to a delay in alignment to the ambient magnetic field and the immobilization (lock-in) of particle moments in sediments due to dewatering and compaction (Verosub, 1977), which induce a possible downward shift of the recorded magnetic features (Roberts and Winklhofer, 2004; Sagnotti et al., 2005; Liu et al., 2008; Mellström et al., 2015). Earlier studies have reported that the paleomagnetic lock-in-depth averaged ~150 years in maar lakes (Stockhausen, 1998).

Anhysteretic Remanent Magnetization (ARM) was produced with an alternating field of 100 mT (therefore hardly mobilizing high-coercivity magnetic minerals) and a bias field of 100 μT. Hence ARM quantifies the concentration of ferromagnetic minerals of low-coercivity such as magnetite. The ratio ARM(30mT)/ARM increases with a decrease of magnetite grain size, when magnetite constitutes the main carrier of the magnetic signal (Nizou et al., 2016).

Isothermal Remanent Magnetization (IRM) is measured after the pulse at 3 T (i.e., IRM_{3T} targeting high-coercivity minerals), then again at 0.3 T ($IRM_{0.3T}$ so as to mobilize solely low-coercivity minerals) in the opposite direction using a pulse magnetizer. Once all the samples were analyzed, the S_{ratio} parameter was determined by calculation to examine characteristics of the magnetic assemblage. In particular, the S_{ratio} shows the relative contributions of low- (between 0 and 0.3 T) and high-coercivity magnetic minerals (between 0.3 and 3 T), and therefore allows estimation of their relative proportions (Bloemendal et al., 1992):

$$S_{ratio} = \frac{1}{2}\left(1 - \frac{IRM_{-0.3T}}{IRM_{3T}}\right) \quad (1)$$

Equations (1) and (2): is it possible to center these two equations in the middle of the page?

An S_{ratio} close to 1 indicates a low relative concentration of magnetite (i.e., low-coercivity minerals). Conversely, a weak S_{ratio} documents a relative concentration increase in hematite (high-coercivity minerals). In addition, High Isothermal Remanent Magnetization (HIRM) was calculated in order to quantify concentrations of high-coercive magnetic minerals (e.g., hematite) in the sediments, independently of the concentrations of low-coercive minerals (Maher and Dennis, 2001; Liu et al., 2007):

$$HIRM = \frac{IRM_{3T} - IRM_{0.3T}}{2} \quad (2)$$

Since it is known that (even at 3 T) magnetic minerals may not be completely magnetically saturated (Rochette et al., 2005) and that atomic substitutions may affect coercivity spectra (Liu et al., 2007), the S_{ratio} and HIRM are not purely quantitative. Nevertheless, we consider, as is typically done, that in our study focused on sediments these parameters are good indicators of variations in low- and high-coercivity magnetic components throughout the sedimentary record. Three additional measurements of IRM stepwise thermal demagnetization were carried out on core Ala-04 (Supplementary Fig. S1). Two heating cycles were conducted at 400 °C and 620 °C, respectively. The first cycle has a reversible curve, which indicates that no mineralogical transformation occurred during heating and cooling at low temperature. The second cycle (also reversible) shows a sharp decline at 580 °C corresponding to the Curie temperature of the magnetite. It confirms that magnetite dominates the κ_{LF} and that it is the main ferromagnetic phase in the sediments. A complementary hysteresis analysis further shows that the magnetic fabric is primarily composed of magnetite grains from multiple domains (Supplementary Fig. S2). Note, however, that the Ala04–36 sample reveals slightly coarser grains (i.e., lower Bcr/Bc ratio). This straightforward interpretation based on the Day diagram is only valid for samples characterized by a unique grain size class of magnetites, and may be rather different in the case of grain size mixing, as often occurs in lake sediments (Dunlop, 2002).

The clastic sediment component (expressed in %) was calculated based on loss-on-ignition or LOI ($LOI_{550°C}$: exposure time 4 h and $LOI_{925°C}$: exposure time 12 h) analyses conducted at CEREGE, and represents the remaining fraction after subtracting organic matter (%OM) and carbonates (%CO_2 was converted to carbonates by multiplying %CO_2 values by 2.27). LOI can be used as an inverse indicator of the minerogenic sedimentation (Nesje et al., 2000; Sandvold et al., 2001; Støren et al., 2008); however, low LOI values (< 5%) have limitations for glacier-fed lake reconstructions due to a low signal-to-nose ratio (Bakke et al., 2005). LOI analyses were performed on the same subsamples as used for the rock magnetic data. We consider biogenic silica concentrations to be negligible since no diatom frustules were found on selected smear slides of core Ala-04.

3.3. X-Ray fluorescence logging

The elemental composition of the sediments was measured at GFZ Potsdam on the split-core surface using an ITRAX micro X-Ray fluorescence (μ-XRF) spectrometer. A chromium tube, which is sensitive for lighter elements, was used with a 30 kV voltage and 30 mA current; the step size was 2 mm and exposure time was 10 s per step. The main elements representing the lithology of the Ala Kol sediments (Ca, Si, Sr, Ti, Fe) were selected for interpretation. The XRF data are displayed as count rates (counts per seconds, or cps) or as elemental ratios. The elemental data presented here have been normalized by incoherent (inc) and coherent (coh) scatters in order to minimize the effects of organic and water contents (Kylander et al., 2011; Davies et al., 2015). The XRF element scanning data fingerprint the mineralogical composition of the sediments. The terrestrial siliciclastic component (e.g., quartz, feldspars, clay minerals) is inferred from Ti, Ca, Sr, Fe, and Si values. In view of the dominant lithologies in the catchment of Lake Ala Kol, including the Takur Tor glacier basement rock (e.g., granodorites, granites and leucogranites), we consider that these five elements are good indicators of detrital input into the lake. The lithogenic elements Si and Ti are geochemically stable, hosted by resistant minerals (such as quartz for Si or titanite or rutile for Ti), and conservative in most geochemical environments (Boës et al., 2011). Ti is widely used as a proxy for catchment erosion. Although it commonly occurs associated with silts in Fe-rich clastic mineral particles (e.g., Ti-oxides and/or Ti-rich magnetites), Ti is also often common in clay minerals. Si occurs in many aluminosilicate minerals (especially alkali feldspars) and quartz, but is also associated with diatom productivity. However, no diatom frustules were found in selected samples analyzed for smear slide observations downcore. Based on good correlations with Ti (Supplementary Fig. S3) and Fe, we infer that Si behaviour is mainly controlled by silicate sources. Moreover, since the lake catchment is endogenic and contains a large proportion of granodiorites and granites (incorporating quartz), we use Si (Si/inc + coh) rather than Ti as a proxy for catchment abrasion. Ca and Sr have both allogenic (detrital input) and authigenic sources in lake sediments (Arnaud et al., 2005). The strong correlation between Ca (and Sr) with pure detrital elements such as Si, Ti and Fe (Supplementary Fig. S3) suggests that Ca and Sr are associated with silicates, particularly plagioclase feldspars, and therefore reflect terrestrial supply to the lake. Increased detrital input as well as reduced organic matter abundance (based on higher Si/inc + coh and Ca/inc + coh where inc + coh is used to minimize the effects of organic carbon content) in proglacial lakes could indeed be related to enhanced glacial activity (Bakke et al., 2010; van der Bilt et al., 2015).

3.4. Chronology

The age-depth model of core Ala-04 was based on both paleomagnetic directions and short-lived radionuclide measurements (^{210}Pb, ^{241}Am, ^{137}Cs) using the clam R package with a smooth spline curve (Blaauw, 2010). The short-lived radionuclide analyses in the upper 6 cm (15 samples) were analyzed using high-efficiency, very low-background, well-type germanium detectors at the Modane

Underground Laboratory. The sampling interval was every 5-mm. ^{137}C was introduced into the environment in 1952–1953 CE as a by-product of atmospheric nuclear weapon tests (with a notable peak at 1963 CE). ^{210}Pb excess (^{210}Pb$_{ex}$) was calculated as the difference between total ^{210}Pb and ^{226}Ra activities (Goldberg, 1963). We then used the Constant Flux/Constant Sedimentation (CFCS) model applied to ^{210}Pb$_{ex}$ to determine mean sedimentation rates (Goldberg, 1963). The age model based on short-lived radionuclides was computed with the serac R package (https://github.com/rosalieb/serac).

4. Results

4.1. Lithology

Sediment core Ala-04 does not show any disturbance (e.g., tilting of sedimentary layers, hiatus). LOI$_{550}$ analyses show that the organic matter content is relatively low in core Ala-04 (mean/max values 3.3% and 6.33%, respectively; mean CaO value: 1.73%) (Supplementary Fig. S4). LOI$_{550}$ is therefore regarded as a proxy for minerogenic dilution in this study. Sediments in core Ala-04 are angular to sub-rounded silts and fine sands, suggesting that most of the material is detrital and minerogenic in origin. Sediments are alternatively homogeneous and laminated downcore, and display numerous black millimeter-scale layers, especially in the upper and lower part of the core (Fig. 2). Sediments mostly alternate between light and dark grey with yellowish grey intervening layers. In the upper part, a 2.5 cm-thick oxidized layer caps the core. The absence of graded sequences in core Ala-04 excludes the interpretation of instantaneous deposition during high-energy precipitation events and suggests, instead, a progressive and continuous clastic sediment supply of glacigenic origin. Thus, we ascribe hereafter the silty sediments of core Ala-04 to glacial flour.

4.2. Geochronology

4.2.1. Short-lived radionuclides

The downcore ^{210}Pb$_{ex}$ profile plotted on a logarithmic scale shows a regular decrease with a mean accumulation rate of 0.056 ± 0.5 cm.yr^{-1} over the upper 5.5 cm of the core (Fig. 2A). The age model derived from the CFCS model is used to provide a continuous age-depth relationship over the upper 5.5 cm. The ^{137}Cs and ^{241}Am activity profiles (Fig. 2A) present a well-defined peak at 3 cm (183.6 ± 3.67 mBq kg^{-1}) and 2.5 cm (5.08 ± 0.68 mBq kg^{-1}), respectively, corresponding to the maximum nuclear weapon testing in the Northern Hemisphere in 1963 CE (Appleby et al., 1991). This peak is in good agreement with the CFCS model (Fig. 2B). Note that the Chernobyl event (1986 CE) is not recorded in the core. Indeed, both the presence of ^{241}Am in the sediments and the location of Lake Ala Kol in

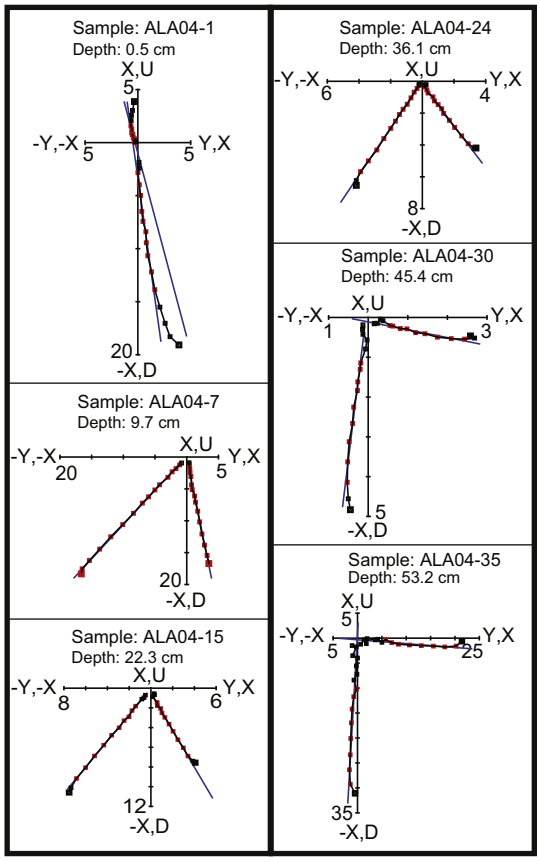

Fig. 3. Selected orthogonal projections of stepwise NRM AF demagnetization for selected samples. The pattern shows that a stable magnetization pointing toward the origin is reached after few steps of AF demagnetization. Units are in mA/m. As the core is only vertically oriented, the X axis of the orthogonal projection corresponds to the insertion direction of the cubes when the sediment was sampled. The vertical axis (up and down) corresponds to the vertical axis of the core.

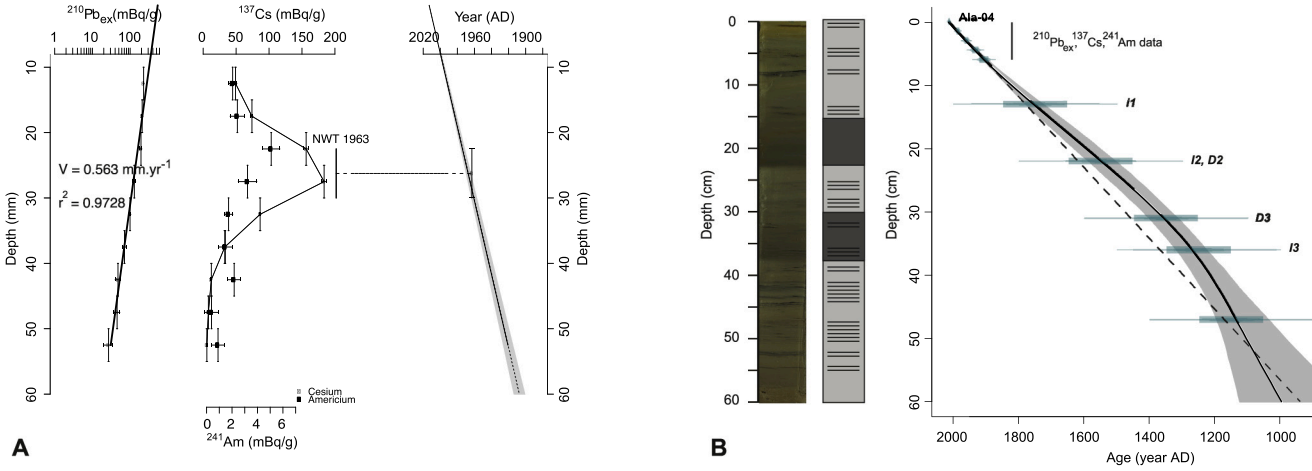

Fig. 2. Age-depth model for the Lake Ala Kol sediment core Ala-04 (photograph and log) including (A) short-lived radionuclides (^{210}Pb$_{ex}$ and ^{137}Cs) with application of the CFCS model to the ^{210}Pb$_{ex}$ profile. (B) Age-depth model for core Ala-04 based on short-lived radionuclides and the PSV data processed with the clam R package using a smooth spline curve. Green lines and rectangles correspond to 95% and 68% confidence intervals, respectively. The dashed line corresponds to the CFCS model (^{210}Pb$_{ex}$ data) extrapolated downcore in Ala-04, for comparison with the PSV-based age model (see Fig. 4). (For interpretation of the references to colour in this figure legend, the reader is referred to the web version of this article.)

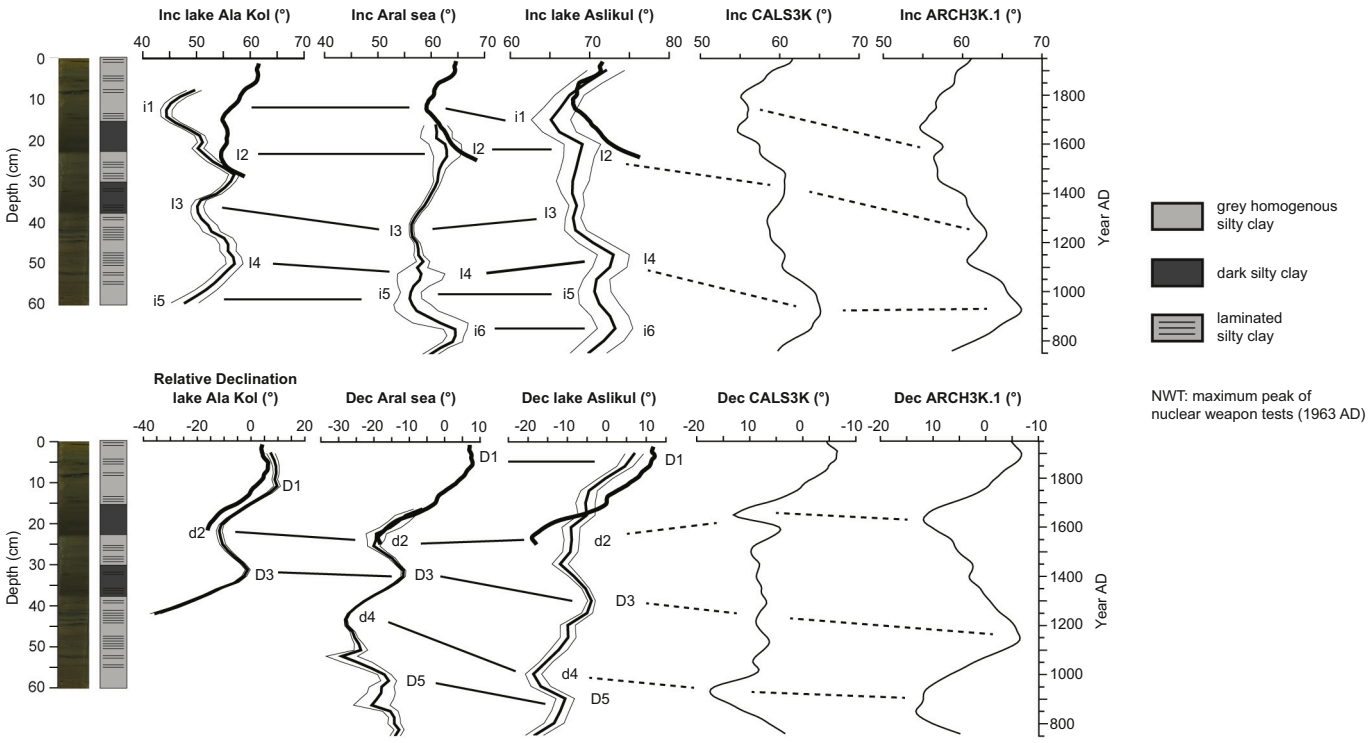

Fig. 4. Paleomagnetic secular variations (PSV). Paleomagnetic data have been plotted as mean values of 40-year intervals, and contours of 95% circles of confidence. Thick black lines for inclination and declination data correspond to historical observations of the magnetic field between 1590 and 1990 CE modelled for the three localities (Lake Ala Kol, Aral Sea, Lake Aslikul). PSV data from Lake Ala Kol (plotted versus depth) are compared with natural archives from Aral Sea (Nourgaliev et al., 2003) and Lake Aslikul (Nourgaliev et al., 1996, 2000), the spherical harmonic GUFM1 model (Jackson et al., 2000), the ARCH3k.1 and CALSK3k.4 models (Korte et al., 2009, 2011). The GUFM1, ARCH3k.1 CALSK3k.4 curves were modelled for our site location (N42°19′03.7″; E78°32′59.5″). All reference curves are plotted versus age. Note that PSV data rely exclusively on ChRM inclination and relative declination data (no relative paleointensity, see text for detail).

Central Asia exclude the possibility of attributing the ^{137}Cs peak at 3 cm to the fallout of radionuclides related to the Chernobyl event. The use of the CFCS model combined with ^{137}Cs and ^{241}Am activity profiles suggest that 1 cm is missing from the top of core Ala-04, most likely due to a disturbed sediment-water interface (Fig. 2).

4.2.2. PSV data

A highly stable magnetization is obtained after a few steps of alternating field (AF) demagnetization (Fig. 3), allowing the determination of a ChRM with a low Maximum Angular Deviation and pointing toward the origin. ChRM inclination and declination as recorded in Lake Ala Kol are compared with paleomagnetic data from: (1) natural archives (Aral Sea and Lake Aslikul), (2) the GUFM1 model and (3) the ARCH3k.1 and CALS3k.4 models (Fig. 4). The ChRM inclination curve exhibits pronounced variations throughout the core with values fluctuating between 40° and 60°. The declination record was not used in full because it is often affected by various problems such as slight sediment disturbances, which can produce significant deviations of the ChRM declination. The ChRM declination values were reoriented to give a core mean declination of zero (i.e., parallel to the north), which is a more readable way to illustrate relative declination values.

ChRM inclination and relative declination values in core Ala-04 correlate well with all reference curves, but in particular with inclination and declination values from Lake Aslikul and the Aral Sea (both situated in Central Asia) (Fig. 4). ChRM inclination minima and maxima in core Ala-04 are unambiguously identified at 13 cm (1750 ± 50 CE; i1), 22 cm (1550 ± 50 CE; I2), 36 cm (1250 ± 50 CE; I3) and 47 cm (1150 ± 50 CE; I4), whereas ChRM declination minima and maxima are observed at 22 cm (1550 ± 50 CE; d2) and 31 cm (1350 ± 50 CE; D3) (Fig. 4, and Table 1 for the corresponding depths). MAD values, which never exceed 3° with an average of 1.35°, indicate high-quality directional data. The age-depth model for core Ala-04 (Fig. 2B) was then based on short-lived radionuclides for the upper 5.5 cm (Fig. 2A) and the PSV data (Table 1). Based on this age-depth model, core Ala-04 spans the past 1000 years, covering the end of the Medieval Period and the Little Ice Age (LIA) with a relative constant sedimentation rate ranging between 0.08 and 0.044 cm.yr^{-1} (average: 0.060 cm.yr^{-1}) (Table 1). Interestingly, sedimentation rates appear to be higher (i.e., almost two-fold) during the Medieval Period compared to afterwards during the LIA (Table 1), during which low sedimentation rates persisted with little variability.

For the sake of testing the reliability of our PSV-based age model below 5.5 cm, the CFCS model was extrapolated downcore (Fig. 2B). Results show that, despite large chronological uncertainties below I4 in core Ala-04, (1) the two age models are fairly comparable and suggest a ca. 1000 CE (800–1150 CE) age at the base of Ala-04 (thus imparting a good level of confidence to the correlations established with the reference paleomagnetic curves), and (2) no significant distortion affected the age model. In addition, the values calculated for the differences between the PSV-based and extrapolated CFCS models (i.e., the paleomagnetic lock-in-depth) mainly fluctuate between 1 and 5 cm, which correspond to a delay of 30–110 years in our study (Table 1). Hence, our estimated paleomagnetic lock-in-depths are negligible in core Ala-04, and thus cause little spreading of the assigned PSV ages during the last millennium.

4.3. Rock magnetic data

The HIRM curve shows a constant concentration of high coercive minerals (hematite) in core Ala-04 (Fig. 5). The HIRM signal is

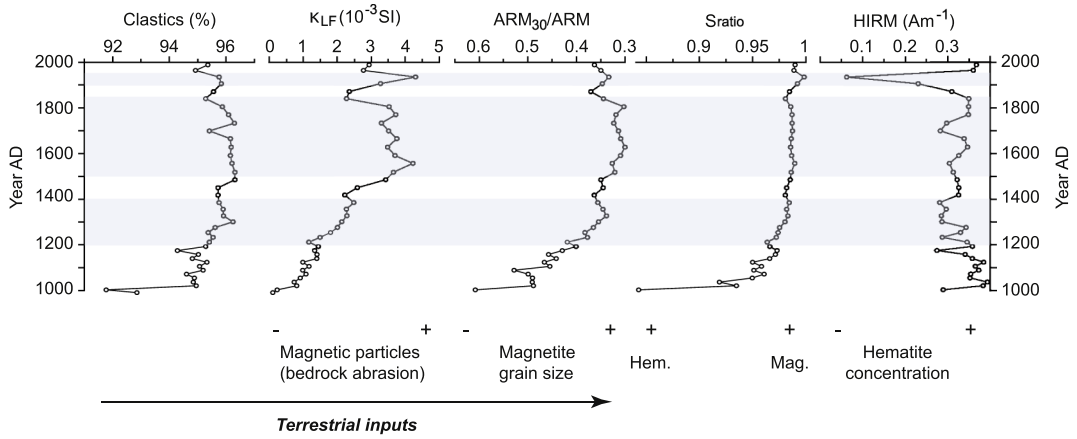

Fig. 5. Rock magnetic and sedimentological proxy data from core Ala-04. See text for interpretation of the different parameters. Grey shadings correspond to increased (and coarser) supply of glaciogenic sediment in core Ala-04 linked with higher glacier abrasion upstream during 1200–1400 CE, 1500–1850 CE and 1900–1950 CE. Hem: Hematite. Mag: Magnetite.

interpreted here as a contribution from a constant source input of distant eolian sediment (hematite being a highly oxidized phase and the most stable phase in long-distance transport). The decrease of HIRM in the topmost sediments just below an oxidized zone is probably linked with diagenetic processes. Our data reveal that the magnetic fabric is constant in core Ala-04, and mainly composed of magnetite judging from persistently high S_{ratio} values (> 0.95) from 1100 CE onwards. Such high S_{ratio} values imply very low relative concentrations of hematite.

Variations of magnetic particle inputs are therefore mainly controlled by variations in magnetite abundance. κ_{LF} is generally high throughout the core (0–5 10^{-3} SI) but shows a prominent and gradual increase between 1000 and 1850 CE (Fig. 5). The highest κ_{LF} values are recorded during the LIA (1500–1850 CE). κ_{LF} declines shortly between 1850 and 1900 CE, followed by a trend to higher values between 1900 and 1950 CE. Alternatively, since magnetite grains predominate in the magnetic assemblage, ARM_{30}/ARM proxy data suggest a gradual increase in magnetite grain size between 1000 and 1850 CE and peak between 1500 and 1850 CE. From 1850 CE onwards, the trend is opposite and exhibit a decrease of magnetite grain size with, however, a small peak around 1950 CE.

4.4. Geochemistry and clastic sediment inputs

Downcore records of clastic sediment, Ca/inc + coh, Si/inc + coh, Sr/inc + coh (not shown) and κ_{LF} all covary throughout most of the sequence. Ca/inc + coh, Si/inc + coh, κ_{LF} and S_{ratio} values are generally low between 1000 and 1200 CE (roughly corresponding to the Medieval Warm Period), although they exhibit a slightly increasing trend that strengthens from 1200 CE onwards. Of interest is a marked decline in Ca/inc + coh and Si/inc + coh values between ca. 1000 and 1050 CE (taken into account the large age uncertainties in this time interval). Clastic sediment concentrations keep increasing from 1200 CE onwards and attain peak values between 1500 and 1850 CE (i.e., the coldest years of the LIA), with however a slight trend toward lower values between ca. 1670 and 1750 CE (Fig. 6). The most recent 250 years of the record exhibit a sharp decline of all parameters during the time span ca. 1850–1900 CE (end of the LIA), which precedes a pronounced increase of clastic abundances (high values of Ca/inc + coh, Si/inc + coh and κ_{LF}) between 1900 and 1950 CE, culminating around 1940 CE. Low detrital inputs characterize the uppermost samples, although this trend is less visible in κ_{LF} and ARM_{30}/ARM proxy data.

5. Discussion

5.1. Sedimentation rates and glacial dynamics

Data from the proximal core Ala-04 in Lake Ala Kol showed that changes in sediment composition were accompanied by varying sedimentation rates during the last millennium, with increased (decreased) sedimentation rates during the Medieval Period (LIA). Such a scenario is paradoxical at a first glance, as one would expect that the amount of glacigenic sediments being transported by meltwater streams would increase during colder and more humid periods (such as the LIA) proportionally to glacier size and thickness (Leonard, 1997). For most temperate glacier systems, enhanced clastic sedimentation in proglacial lakes (and thus higher sedimentation rates) is indeed correlated to multi-decadal and secular-scale phases of glacier advance, rather than recession (Leonard, 1997; Matthews et al., 2000). This is because the large meltwater supply typical of temperate glaciers delivers large amounts of debris from under the ice, resulting in massive sediment accumulation in glacier-fed lacustrine systems (Koppes et al., 2015). The relationship between glacial abrasion and glacigenic (clastic) sediment discharge is, however, different for glacier thermal regimes typical of colder climates (e.g., polar glaciers), such as the Takur Tor glacier located at high altitude in NE Kyrgyzstan. For polar glaciers, glacial erosion is expected to dwindle as surface melting decreases because little or no water attains the glacier bed (without refreezing) to promote glacier sliding and flush out sediment produced from abrasion of the ice-bed surface (Koppes et al., 2015), ultimately limiting the supply of sediments to terminal lacustrine systems. Hence erosion rates for polar glaciers are lower than for temperate glaciers with similar ice discharges, and this is primarily related to the abundance of meltwater accessing the bed (Koppes et al., 2015). Furthermore, colder (warmer) climate conditions foster a prolonged (shortened) freezing period in the lake, which in turn implies that the supply of glacigenic sediment by the subglacial hydrologic system occurs over a shorter (prolonged) period of time in the year. Both of these mechanisms may explain the two-fold lower sedimentation rates in core Ala-04 during the LIA compared to the Medieval Period, involving lower erosion rates generated at the glacier bed during the colder/wetter LIA, less delivery of clastic sediment (during a prolonged freezing period each year) and thus, lower sedimentation rates observed in the lake sediments. It further implies that the Takur Tor glacier upstream from Lake Ala Kol evolved from a temperate regime during the Medieval Period to a polar regime during the LIA (before reversing again to a temperate regime at present).

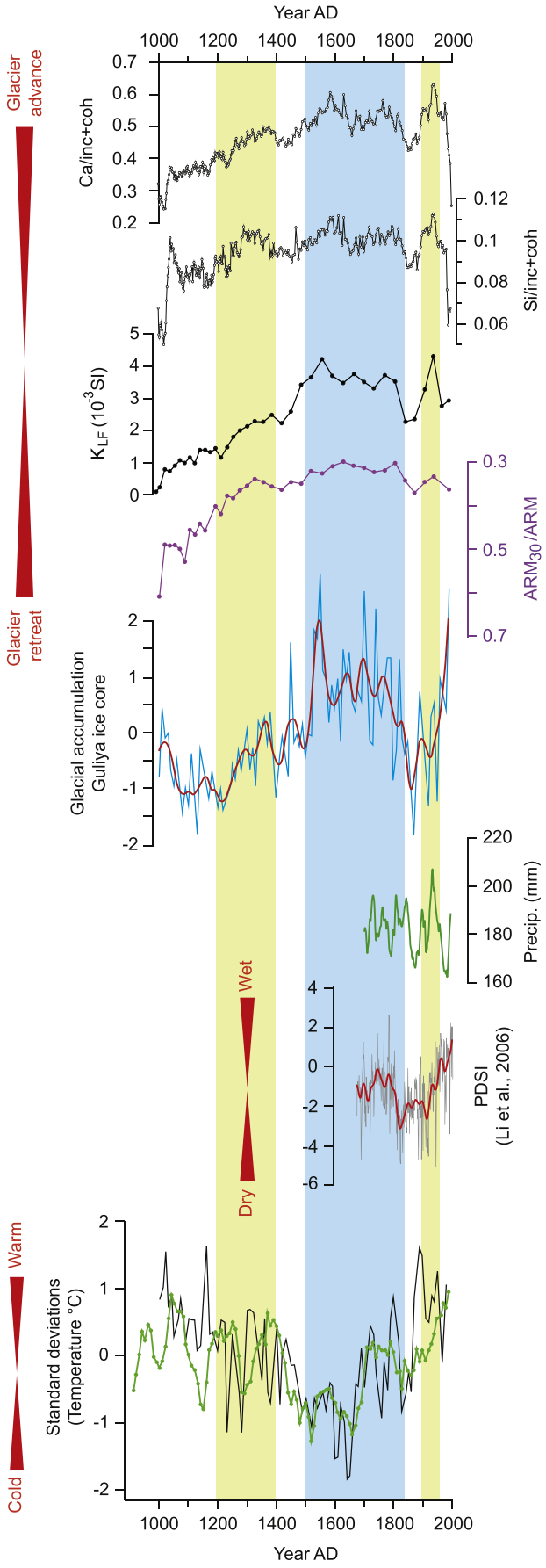

Fig. 6. Glacier fluctuations (advance/retreat) during the last millennium inferred from geochemical (XRF) and rock magnetic proxy data compared with the ice accumulation record of the Guliya Ice Core from the western Kunlun Range (Thompson et al., 1995), the tree-ring based precipitation reconstruction for the Hutubi region on the northern slopes of the central Tian Shan (Chen et al., 2009), the PDSI record (grey line) and its 11-year running average (red bold line) of Li et al. (2006) and the Central Asian tree-ring width composite record (black line; Yang et al., 2009) along with a decadal-resolved mean annual temperature reconstruction for China (green dotted curve; Yang et al., 2002). The Guliya ice record was linearly interpolated to a uniform 10-year interval, standardized to have zero mean and unit standard deviation from 1000 CE onwards, and then arithmetically averaged following Chen et al. (2010). Yellow shadings correspond to glacier expansion during 1200–1400 CE and 1900–1950 CE. Light blue shading refers to the maximal glacial advance during 1500–1850 CE. (For interpretation of the references to colour in this figure legend, the reader is referred to the web version of this article.)

5.2. Proxy-based limnological changes and glacial activity

It is noteworthy that lake coring site Ala-04 is proximal to the Takur Tor glacier (Fig. 1), suggesting that any changes of glacier activity in the catchment are expected to be recorded in the lake sediments, either through changing sedimentation rates and/or sediment grain size. Previous records exhibiting increased abundances of Ti and Si in glacier-fed lakes have been interpreted as reflecting inputs of inorganic detrital material resulting from catchment processes, such as glacier activity and flood events (Bakke et al., 2009; Røthe et al., 2018; Røthe et al., 2015; Fouinat et al., 2017). Moreover, higher abundances of Ti have been directly related to positive glacial mass balance, and thus glacier expansion (Fouinat et al., 2017). In turn, magnetic susceptibility has been recognized as a useful proxy for glacier activity (Liu et al., 2014). These previous works that focus on reconstructing past glacial activity in a lake catchment based on sediment core proxies (although entailing indirect rather than direct evidence for glacier fluctuations) thus substantiate the use of coupled geochemical and rock magnetic data to track past glacier dynamics in the proximal core Ala-04. Therefore, higher κ_{LF} and S_{ratio} values along with high Si/inc + coh and Ca/inc + coh are interpreted to reflect detrital input linked to the intensification of glacier activity in the lake catchment (advance/retreat), and/or enhanced glacier melt and particle transport to the lake. In accordance with this, in proximal settings, higher abundances of coarser (=silt-sized) particles in lake sediments has been related to increased glacial erosion (Matthews et al., 2000; Nesje et al., 2001; Bakke et al., 2005; Liu et al., 2014). Accordingly, here in this study, we use high (low) values of the coarse silt fraction – i.e., low (high) ARM_{30}/ARM in core Ala-04 – to infer periods of glacier advance (retreat) (Fig. 6). Besides increased detrital input, reduced organic matter abundance in proglacial lakes could be related to increased glacial activity (Nesje et al., 1991, 2000; Fouinat et al., 2017). Hence, though LOI variations must be considered with caution in glacier-fed lakes with LOI < 5% (Bakke et al., 2005), high LOI_{550} values (> 3.5%) would indicate a contraction of the glacier upstream from the lake while LOI_{550} < 3.5% would suggest increased glacial extent in the lake catchment (Supplementary Fig. S4). Considering all lines of evidence, the contribution of coarser glacigenic (clastic) sediments was greater during periods of glacial expansion than for period of glacial retreat. Thus high concentrations of Si/inc + coh and Ca/inc + coh coeval with low ARM_{30}/ARM values (coarser magnetites) imply increased glacial activity during periods of glacier expansion (Fig. 6).

5.3. Glacier fluctuation during the past 1000 years

Based on the Lake Ala Kol sedimentary proxies defined above, past changes in the Takur Tor glacier mass balance were reconstructed for the last ca. 1000 years (Fig. 6) with, however, a less robust chronology for the time interval 1000–1200 CE in which large uncertainties are

exhibited in the PSV-based age model (Fig. 4). Three periods of increasing glacier expansion at 1200–1400 CE, 1500–1850 CE and 1900–1950 CE (e.g., high κ_{LF}, Si/inc + coh, Ca/inc + coh and low ARM_{30}/ARM) represent prominent glacier advances; the most significant one (1500–1850 CE) corresponding to the coldest phase of the LIA. The period of maximal glacial extent determined from core Ala-04 during the LIA is in phase with a series of glacial advances in the western Tian Shan (Savoskul and Solomina, 1996; Blomdin et al., 2016) and Pamir Mountains (Liu et al., 2014). In contrast, periods of glacier retreat of the Takur Tor glacier upstream from the lake (e.g., lower κ_{LF} along with higher ARM_{30}/ARM) occurred at 1000–1200 CE, 1400–1500 CE, 1850–1900 CE and 1950–2000 CE. This suggests that cold (and wet) climate conditions were characteristic of the LIA, whereas warm (and probably less humid) conditions prevailed during the Medieval Period, as it was reported elsewhere for high Central Asia (Aichner et al., 2015). Moreover, Lake Ala Kol proxies also reveal climatic changes on decadal time scales with, for instance, an anomalously warm and dry climate between ca. 1000 and 1050 CE (taken into account the large age uncertainties in this time interval). Interestingly, the period 1900–1950 CE suggests glacial expansion while other glaciers in the Tian Shan Mountains were retreating (Kutuzov and Shahgedanova, 2009). One alternative hypothesis to glacier expansion during this time interval would be a temporal lag (i.e., delay) between sediment yield by the glacier and clastic supply to the lake during the late LIA through to temporary sediment storage in the catchment, as already shown in other proglacial lacustrine systems (Navratil et al., 2012; Fouinat et al., 2017). However, further investigation (including field mapping) focused on sediment storage, erosion, availability and delivery to Lake Ala Kol is required in order to better understand the complex detrital input variations at decadal to centennial time scales.

Overall, the Takur Tor glacier fluctuations in the Lake Ala Kol catchment appear to be phase-locked with the Guliya ice core record from the western Kunlun Range, 6200 m.a.s.l (Fig. 6). In particular, glacier advances mirror maximal ice accumulation in the Guliya ice core between 1500 and 1850 CE, although peak accumulation occurs slightly earlier (~50 years) in the Takur Tor during the 20th century glacier advance. The Guliya ice core record has been used to reconstruct both short- and long-term precipitation in Central Asia (Yang et al., 2009). Moreover, a positive correlation was demonstrated between Guliya ice accumulation and precipitation during the period 1950–1989 CE at a meteorological station located in the lowland plains, downstream of Lake Ala Kol (Yang et al., 2009). This suggests that the Guliya ice record can be used as a reliable indicator of precipitation change in central Tian Shan Mountains during the last 1000 years, as also proposed earlier by Wang et al. (2004). In accordance with this, our proxy data from Lake Ala Kol show a close correspondence with a tree-ring based precipitation reconstruction for Central Tian Shan (Chen et al., 2009) (Fig. 6) between 1700 and 2000 CE. Palaeoenvironmental variations inferred from core Ala-04 also match well with the tree-ring based April–June Palmer Drought Severity Index (PDSI) reconstruction for central Tian Shan in China over the last 300 years (Li et al., 2006) (Fig. 6) with, for instance, a generally wet 18th century, a dry 19th century and a conspicuous moisture increase during the early half of the 20th century. Climate anomalies at the pluri-decadal time scale also compare fairly well: (1) a dry period identified between 1670 and 1730 CE in the PDSI reconstruction matches with lower glacial abrasion in core Ala-04; (2) abnormally wet conditions during the 1780–1790s (PDSI) match with a glacier advance in the central Tian Shan dated at 1777 ± 20 CE (Chen, 1988) as well as the Lake Ala Kol record (maximum of Ca/inc + coh); (3) dry conditions recorded in the PDSI between 1820 and 1910 CE are also recorded in Lake Ala Kol by the occurrence of dry years around 1840–1900 CE, while the wettest years are found between 1920 and 1950 CE in all proxies. In general, the palaeoenvironmental variations inferred from core Ala-04 at high altitude in central Tian Shan also coincide well with lowland lake-level fluctuations in Kyrgyzstan during the past 1000 years. In particular, Lake Issyk Kul was 5–8 m above its present level between 1600 and 1800 CE (Giralt et al., 2004), while low lake levels were recorded in Lake Chatyr Kol during the 11th and 16th centuries (Solomina et al., 2004).

Although a good correspondence exists between phases of glacier advance/retreat in central Tian Shan and net accumulation rates in the Guliya ice core, glacier fluctuations (as inferred from core Ala-04) are also in good agreement with temperature changes over the past millennium (Fig. 6). The conformity between proxy data for glacial expansion around Lake Ala Kol, the central Asian tree-ring composite and a decadal-resolved temperature record for China (Yang et al., 2002, 2009) implies that warm conditions prevailed between 1000 and 1200 CE when the Takur Tor glacier regressed upstream from the lake. Coarser detrital input from 1200 CE onwards in core Ala-04 matches with the onset of cold and wet conditions during the LIA and a prominent advance of the Takur Tor glacier in central Tian Shan. This trend was interrupted by a short warmer interval during the 15th century, as already reported elsewhere (Yang et al., 2009). However, there are some notable miscorrelations between the Ala Kol record and temperature reconstructions for Central Asia, while there is a much better correspondence with the Guliya ice core record (indicative of precipitation variations). The most intriguing paradox concerns the LIA. Albeit maximal glacier expansion recorded in core Ala-04 (coevally to highest accumulation rates in the Guliya ice core) between 1500 and 1850 CE, cold conditions as reported from both temperature reconstructions are only observed between 1500 and 1700 CE, thus suggesting that temperature is likely not the primary parameter controlling glacial dynamics at high altitudes and in dry areas. Another significant mismatch occurs during the 13th–14th centuries when increased glacier advance in the Ala Kol catchment concurred with enhanced accumulation rates (and thus higher precipitation) in the Guliya ice core, while temperatures were generally high. Given all these lines of evidence, the Ala Kol record exhibits a better correspondence with the precipitation-sensitive Guliya ice core record than with temperature changes alone, on both decadal and centennial timescales.

This observation is in agreement with recent temperature and precipitation anomalies measured in meteorological stations from high central Tian Shan (Chatir Kol, Koilu and Tian Shan; Kyrgyzstan), located in the vicinity of Lake Ala Kol (Fig. 7). All three stations show a similar annual cycle, in which more than 80% of annual precipitation falls during late spring and summer (April–September). Thus, in high central Tian Shan, the seasons of highest glacier accumulation and ablation are close or even coeval. Interestingly, although both summer precipitation and air temperature are closely related for the period 1950–1990 CE (i.e., the time interval comparable for the three stations), standardized values show that summer precipitation anomalies slightly exceed those of summer air temperature, except for 1978 and 1984 CE when particularly hot summers were recorded. However, strong temperature anomalies can be observed from 1990 CE onwards (Tian Shan station) including the recent unprecedented warming that led to strong glacier mass loss (Narama et al., 2009; Dehecq et al., 2018). Instrumental data show thus that, although increasing summer temperatures seem to be the dominant factor affecting recent glacier shrinkage in the Pamir Mountains and part of the Tian Shan (Narama et al., 2009; Chen et al., 2016), summer air temperatures may not have been the main climatic driver of glacier accumulation in high central Tian Shan. Indeed, instrumental data from NE Kyrgyzstan (Fig. 7) suggest that annual precipitation variations have exceeded changes in summer air temperature at least during the last century. Our proxy-based record further suggests that precipitation primarily controlled glacier dynamics at high altitude sites in the central Tian Shan during the last millennium, and that precipitation changes also need to be considered as an important driver of glacial mass balance at centennial to millennial time scales.

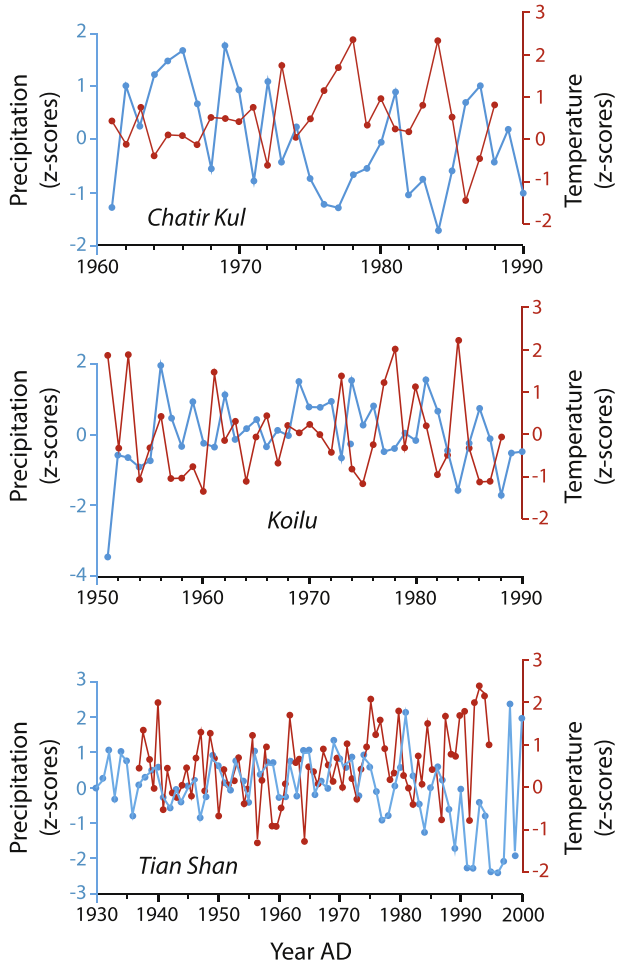

Fig. 7. Summer precipitation (April–September; full line) and temperature (May–August; dashed line) anomalies from three meteorological stations in central Tian Shan (Chatir Kul, Koilu and Tian Shan). Precipitation and temperature anomalies are shown as standardized values expressed in unit of standard deviation (i.e., standardized to have zero mean and a standard deviation of 1). Precipitation and temperature data originate from Williams and Konovalov (2008).

6. Conclusions

A 60-cm sediment core from Lake Ala Kol (Ala-04), a high-altitude glacier-fed lake (Takur Tor glacier, NE Kyrgyzstan) was analyzed to generate a continuous and high-resolution record of palaeoenvironmental change and glacial fluctuations in central Tian Shan for the last millennium. Core Ala-04 provides evidence for three periods of glacier expansion during 1200–1400 CE, 1500–1850 CE and 1900–1950 CE based on high κ_{LF}, Si/inc + coh, Ca/inc + coh and low ARM_{30}/ARM values, the most prominent of which was recorded during the coldest years of the Little Ice Age (1500–1850 CE). Episodes of glacier advance for the Takur Tor are concomitant with a series of glacier expansions reported elsewhere in the Tian Shan and Pamir Mountains during the LIA. Moreover, the timing of glacier advance and retreat in the catchment of Lake Ala Kol closely matches variations in ice accumulation in the Guliya ice core during the last 1000 years, suggesting a strong relationship between precipitation changes and glacial accumulation/ablation dynamics in central Tian Shan on centennial to sub-millennial time scales. Alternatively, the reconstructed glacier dynamics are in relatively good agreement with temperature changes in the region, although mismatches occurred especially during the LIA. These results also suggest that precipitation variations, rather than temperatures, are the primary driver of glacier fluctuations during the study period. This pilot investigation represents one of the first paleolimnological studies of past glacial activity in the Tian Shan Mountains from high Central Asia. Located near the boundary between winter- versus summer-dominated precipitation regimes in Kyrgyzstan, glaciers in the high Tian Shan may have responded in a complex way to temperature and precipitation during the last millennium. Forthcoming studies should help to obtain a broader picture of the past glacier dynamics in the Tian Shan Mountains, which could be integrated with those available from the Pamir and the Kunlun mountain ranges.

Supplementary data to this article can be found online at https://doi.org/10.1016/j.palaeo.2020.109987.

Acknowledgements and funding

We warmly thank Matthew Makou (LGL-TPE, ENS Lyon) for his precious language editing of the manuscript. We also acknowledge Andrew Jackson (ETH Zürich), Monika Korte (GFZ Potsdam, Germany) and Danis Nourgaliev (University of Kazan, Russia) for providing the paleomagnetic data in their respective database. We are grateful to Gilles Escarguel (LGL-TPE, France) for his precious insights regarding statistical analyses on the instrumental data. We also thank Rik Tjallingii and Jens Mingram (GFZ Potsdam, Germany) for performing the XRF measurements, and Doriane Delanghe (CEREGE, France) for conducting the LOI analyses. We thank Christian Marshall for technical support in the field. Aijan Ainabekova (CAIAG Bishkek, Kyrgyzstan) and Ermek Baibagyshov (Kyrgyz National University of Naryn, Kyrgyzstan) are gratefully acknowledged for their partnership and precious help regarding administrative issues. The coring expedition was co-funded by the Fédération de Recherche ECCOREV (project KLAP2). E.B. received the support of a fellowship from “la Caixa” Foundation (ID100010434). The fellowship code is LCF/BQ/PR19/11700001. The authors thank the Laboratoire Souterrain de Modane (LSM) facilities for the gamma spectrometry measurements. We finally thank four anonymous reviewers for their constructive comments that helped to improve the manuscript.

Declaration of Competing Interest

The authors declare that they have no known competing financial interests or personal relationships that could have appeared to influence the work reported in this paper.

References

Aichner, B., Feakins, S.B., Lee, J.E., et al., 2015. High-resolution leaf wax carbon and hydrogen isotopic record of the late Holocene paleoclimate in arid Central Asia. Clim. Past 11, 619–633.
Aizen, E.M., Aizen, V.B., Melack, J.M., et al., 2001. Precipitation and atmospheric circulation patterns at mid-latitudes of Asia. Int. J. Climatol. 21, 535–556.
Aizen, V.B., Aizen, E.M., Melack, J.M., et al., 1997. Climatic and hydrologic changes in the Tian Shan, Central Asia. J. Clim. 10, 1393–1404.
Appleby, P.G., Richardson, N., Nolan, P.J., 1991. ^{241}Am dating of lake sediments. Hydrobiologia 214, 35–42.
Arnaud, F., Revel, M., Chapron, E., et al., 2005. 7200 years of Rhône river flooding activity in Lake Le Bourget, France: a high-resolution sediment record of NW Alps hydrology. Holocene 15 (3), 420–428.
Bakke, J., Lie, Ø., Nesje, A., et al., 2005. Utilizing physical sediment variability in glacier-fed lakes for continuous glacier reconstructions during the Holocene, Northern Folgefonna, Western Norway. Holocene 15 (2), 161–176.
Bakke, J., Lie, O., Heegaar, E., et al., 2009. Rapid oceanic and atmospheric changes during the Younger Dryas cold period. Nat. Geosci. 2, 202–205.
Bakke, J., Dahl, S.O., Paasche, Ø., et al., 2010. A complete record of Holocene glacier variability at Austre Okstindbreen, Northern Norway: an integrated approach. Quat. Sci. Rev. 29, 1246–1262.
Blaauw, M., 2010. Methods and code for ‘classical’ age-modelling of radiocarbon sequences. Quat. Geochronol. 5 (5), 512–518.
Bloemendal, J., King, J.W., Hall, F.R., 1992. Rock magnetism of Late Neogene and Pleistocene deep sea sediments: relationship to sediment source, diagenetic processes, and sediment lithology. J. Geophys. Res. Solid Earth 97, 4361–4375.
Blomdin, R., Stroeven, A.P., Harbor, J.M., et al., 2016. Evaluating the timing of former glacier expansions in the Tian Shan: a key step towards robust spatial correlations. Quat. Sci. Rev. 153, 78–96.

Boës, X., Rydberg, J., Martinez-Cortizas, A., et al., 2011. Evaluation of conservative lithogenic elements (Ti, Zr, Al, and Rb) to study anthropogenic element enrichments in lake sediments. J. Paleolimnol. 46, 75–87.
Böhner, J., 2006. General climatic controls and topoclimatic variations in central and high Asia. Boreas 35, 279–295.
Bolch, T., 2007. Climate change and glacier retreat in northern Tien Shan (Kazakhstan/Kyrgystan) using remote sensing data. Glob. Planet. Chang. 56, 1–12.
Chen, F., Yuan, Y.J., Wei, W.S., et al., 2009. Reconstruction and analysis of precipitation of the basin of Hutubi river in middle Tianshan mountains during the last 313 years. Arid Zone Res. 26, 130–135.
Chen, F.H., Chen, J.H., Holmes, J., et al., 2010. Moisture changes over the last millennium in arid Central Asia: a review, synthesis and comparison with monsoon region. Quat. Sci. Rev. 29, 1055–1068.
Chen, J.Y., 1988. Preliminary studies on using lichen dating to study Holocene glacial changes in the source region of Urumqi River, Tian Shan (in Chinese). Sci. Chin. B 1, 95–104.
Chen, Y., Li, W., Deng, H., et al., 2016. Changes in Central Asia's water tower: past, present and future. Sci. Rep. https://doi.org/10.1038/srep35458.
Davies, S.J., Lamb, H.F., Roberts, S., 2015. Micro-XRF core scanning in palaeolimnology: recent developments. In: Croudace, I., Rothwell, R. (Eds.), Micro-XRF Studies of Sediment Cores. Developments in Paleoenvironmental Research. 17 Springer, Dordrecht.
Dehecq, A., Gourmelen, N., Gardner, A.S., et al., 2018. Twenty-first century glacier slowdown driven by mass loss in high mountain Asia. Nat. Geosci. 12, 22–27.
Dunlop, D.J., 2002. Theory and application of the Day plot (M_{rs}/M_s versus H_{cr}/H_c) 2. Application to data for rocks, sediments, and soils. J. Geophys. Res. 107 (B3). https://doi.org/10.1029/2001JB000487.
Fouinat, L., Sabatier, P., Poulenard, J., et al., 2017. One thousand seven hundred years of interaction between glacial activity and flood frequency in proglacial Lake Muzelle (Western French Alps). Quat. Res. 87, 407–422.
Giralt, S., Ramon, J., Klerkx, J., et al., 2004. 1000 year of environmental history of Lake Issyk Kul. In: Nihoul, J.C., Zavialov, P., Micklin, P.P. (Eds.), Dying and Dead Seas: Climatic versus Anthropic Causes. Springer, Dordrecht, pp. 253–285.
Goldberg, E.D., 1963. Geochronology with ^{210}Pb Radioactivity Dating. International Atomic Energy Agency, Vienna, pp. 121–131.
IPCC, 2013. Climate Change 2013: The Physical Science Basis. Contribution of Working Group I to the Fifth Assessment Report of the Intergovernmental Panel on Climate Change. Cambridge University Press, Cambridge, United Kingdom and New York, NY, USA, pp. 1535.
Jackson, A., Jonkers, A.R.T., Walker, M.R., 2000. Four centuries of geomagnetic secular variation from historical records. Philos. Trans. R. Soc. A Math. Phys. Eng. Sci. 358, 957–990.
Kirschvink, J.L., 1980. The least-squares line and plane and the analysis of palaeomagnetic data. Geophys. J. R. Astron. Soc. 62, 699–718.
Koppes, M., Hallet, B., Rigmot, E., et al., 2015. Observed latitudinal variations in erosion as a function of glacier dynamics. Nature 526. https://doi.org/10.1038/nature15385.
Korte, M., Donadini, F., Constable, C.G., 2009. Geomagnetic field for 0–3 ka: 2. A new series of time-varying global models. Geochem. Geophys. Geosyst. https://doi.org/10.1029/2008GC002297.
Korte, M., Constable, C., Donadini, F., et al., 2011. Reconstructing the Holocene geomagnetic field. Earth Planet. Sci. Lett. 312, 497–505.
Kutuzov, S., Shahgedanova, M., 2009. Glacier retreat and climatic variability in the eastern Terskey–Alatoo, inner Tien Shan between the middle of the 19th century and beginning of the 21st century. Glob. Planet. Chang. 69, 59–70.
Kylander, M.E., Ampel, L., Wohlfarth, B., al., 2011. High-resolution X-Ray fluorescence core scanning analysis of Les Echets (France) sedimentary sequence: new insights from chemical proxies. J. Quat. Sci. 26 (1), 109–117.
Leonard, E.M., 1997. The relationship between glacial activity and sediment production: evidence from a 4450-year varve record of neoglacial sedimentation in Hector Lake, Alberta, Canada. J. Paleolimnol. 17, 319–330.
Li, J., Gou, X., Cook, E.R., et al., 2006. Tree-ring based drought reconstruction for the central Tien Shan area in Northwest China. Geophys. Res. Lett. 33, L07715. https://doi.org/10.1029/2006GL025803.
Liu, Q., Roberts, A.P., Torrent, J., et al., 2007. What do the HIRM and S-ratio really measure in environmental magnetism. Geochem. Geophys. Geosyst. https://doi.org/10.1029/2007GC001717.
Liu, Q.S., Roberts, A.P., Rohling, E.J., et al., 2008. Post-depositional remanent magnetization lock-in and the location of the Matuyama-Brunhes geomagnetic reversal boundary in marine ad Chinese loess sequences. Earth Planet. Sci. Lett. 275, 102–110.
Liu, X., Herzschuh, U., Wang, Y., et al., 2014. Glacier fluctuations of Muztagh Ata and temperature changes during the late Holocene in westermost Tibetan Plateau, based on glaciolacustrine sediment records. Geophys. Res. Lett. 41, 6265–6273.
Lurcock, P.C., Wilson, G.S., 2012. PuffinPlot: a versatile, user-friendly program for paleomagnetic analysis. Geochem. Geophys. Geosyst. 13. https://doi.org/10.1029/2012GC004098.
Maher, B.A., Dennis, P.F., 2001. Evidence against dust-mediated control of glacial–interglacial changes in atmospheric CO 2. Nature 411. https://doi.org/10.1038/35075543.
Matthews, J.A., Olaf Dahl, S., Nesje, A., et al., 2000. Holocene glacier variations in central Jotunheimen, Southern Norway based on distal glaciolacustrine sediment cores. Quat. Sci. Rev. 19, 1625–1647.
Mellström, A., Nilsson, A., Stanton, T., et al., 2015. Post-depositional remanent magnetization lock-in-depth in precisely dated varved sediments assessed by archaeomagnetic field models. Earth Planet. Sci. Lett. 410, 186–196.
Narama, C., Shimamura, Y., Nakayama, D., et al., 2006. Recent change of glacier coverage in the western Terskey-Alatoo range, Kyrgyz Republic, using Corona and Landsat. Ann. Glaciol. 43, 223–229.
Narama, C., Kääb, A., Duishonakunov, M., et al., 2009. Spatial variability of recent glacier area changes in the Tien Shan mountains, Central Asia, using Corona (~1970), Landsat (~2000) and ALOS (~2007) satellite data. Glob. Planet. Chang. 71 (1–2), 42–54.
Navratil, O., Evrard, O., Esteves, M., et al., 2012. Temporal variability of suspended sediment sources in an alpine catchment combining river/rainfall monitoring and sediment fingerprinting. Earth Surf. Process. Landf. 37, 828–846.
Nesje, A., Kvamme, M., Rye, N., et al., 1991. Holocene glacial and climate history of the Jostedalsbreen region, western Norway; evidence from lake sediments and terrestrial deposits. Quat. Sci. Rev. 10, 87–114.
Nesje, A., Dahl, S.O., Andersson, C., et al., 2000. The lacustrine sedimentary sequence in Sygneskardvatnet, western Norway: a continuous, high-resolution record of the Jostedalsbreen ice cap during the Holocene. Quat. Sci. Rev. 19, 1047–1065.
Nesje, A., Matthews, J.A., Dahl, S.O., et al., 2001. Holocene glacier fluctuations of Flatebreen and winter-precipitation changes in the Jostedalsbreen region, Western Norvay, based on glaciolacustrine sediment records. Holocene 11, 267–280.
Niederer, P., Bilenko, V., Ershove, N., et al., 2007. Tracing glacier wastage in the Northern Tien Shan (Kyrgyzstan/Central Asia) over the last 40 years. Clim. Chang. 86, 227–234.
Nikonorov, V.V., Karaev, J.V., Zamaletdinov, T.S., et al., 2000. Explanatory Notes and Catalogue of Mineral Deposits Shown on the Map of Mineral Resources of the Kyrgyz Republic, Scale 1:1,000,000. Bishkek. pp. 75.
Nizou, J., Demory, F., Dubrulle-Brunaud, C., 2016. Monitoring and dredged-dumped sediment dispersal off the Bay of Seine (Northern France) using environmental magnetism. C.R. Geosci. 348, 451–461.
Nourgaliev, D.K., Borisov, A., Heller, F., et al., 1996. Geomagnetic secular variations through the last 3500 years as recorded by lake Aslikul sediments from Eastern Europe (Russia). Geophys. Res. Lett. 23, 375–378.
Nourgaliev, D.K., Heller, F., Burov, B., et al., 2000. Variation of geomagnetic field elements for the last 4000 years from paleomagnetic investigations of Lake Aslikul (South – West Bashkiriya) (in Russian). Geomagn. Aeron. 40 (4), 97–106.
Nourgaliev, D.K., Heller, F., Borisov, A.S., et al., 2003. Very high resolution paleosecular variation record for the last ~1200 years from the Aral Sea. Geophys. Res. Lett. 30. https://doi.org/10.1029/2003GL018145.
Peel, M.C., Finlayson, B.L., Mcmahon, P.A., 2007. Updated world map of the Köppen-Geiger climate classification. Hydrol. Earth Syst. Sci. 4, 439–473.
Roberts, A.P., Winklhofer, M., 2004. Why are geomagnetic excursions not always recorded in sediments? Constraints from post-depositional remanent magnetization lock-in modelling. Earth Planet. Sci. Lett. 227, 345–359.
Rochette, P., Mathé, P.E., Esteban, L., et al., 2005. Non-saturation of the defect moment of goethite and fine-grained hematite up to 57 Teslas. Geophys. Res. Lett. 32, L22309. https://doi.org/10.1029/2005GL024196.
Røthe, T.O., Bakke, J., Vasskog, K., et al., 2015. Arctic Holocene glacier fluctuations reconstructed from lake sediments at Mitrahalvøya, Spitsbergen. Quat. Sci. Rev. 109, 111–125.
Røthe, T.O., Bakke, J., Støren, E.W.N., et al., 2018. Reconstructing Holocene glacier and climate fluctuations from lake sediments in Vårfluesjøen, Northern Spitsbergen. Front. Earth Sci. 6. https://doi.org/10.3389/feart.2018.00091.
Sagnotti, L., Budillon, F., Dinarès-Turell, J., et al., 2005. Evidence for a variable paleomagnetic lock-in-depth in the Holocene sequence from the Salerno Gulf (Italy): implications for "high-resolution" paleomagnetic dating. Geochem. Geophys. Geosyst. https://doi.org/10.1029/2005GC001043.
Sandvold, S., Lie, Ø., Nesje, A., Dahl, S.O., 2001. Holocene glacial and colluvial activity in Leirungsdalen, eastern Jotunheimen, south–central Norway. Norsk Geologisk Tidsskrift 81, 25–40.
Savoskul, O.S., 1997. Modern and little ice age glaciers in "humid" and "arid" areas of the Tien Shan, Central Asia: two different patterns of fluctuation. Ann. Glaciol. 24, 142–147.
Savoskul, O.S., Solomina, O.N., 1996. Late Holocene glacier variations in the frontal and inner ranges of the Tien Shan, Central Asia. The Holocene 6 (1), 25–35.
Solomina, O.N., Barry, R., Bodnya, M., 2004. The retreat of Tien Shan glaciers (Kyrgyzstan) since the Little Ice Age estimated from aerial photographs, lichenometric and historical data. Geogr. Ann. 86A, 205–215.
Sorg, A., Bolch, T., Stoffel, M., et al., 2012. Climate change impacts on glaciers and runoff in Tien Shan (Central Asia). Nat. Clim. Chang. 2, 725–731.
Spassov, S., Valet, J.P., 2012. Detrital magnetizations from redeposition experiments of different natural sediments. Earth Planet. Sci. Lett. 351, 147–157.
Stockhausen, H., 1998. Geomagnetic palaeosecular variation (0–13,000 yr BP) as recorded in sediments from three maar lakes from the West Eifel (Germany). Geophys. J. Int. 135, 898–910. https://doi.org/10.1046/j.1365-246X.1998.00664.x.
Stoner, J.S., St-Onge, G., 2007. Chapter three magnetic stratigraphy in paleoceanography: reversals, excursions, paleointensity, and secular variation. In: Hillaire-Marcel, C., De Vernal, A. (Eds.), Developments in Marine Geology, Proxies in Late Cenozoic Paleoceanography. Elsevier, pp. 99–138.
Støren, E.N., Dahl, S.O., Lie, Ø., 2008. Separation of late-Holocene episodic paraglacial events and glacier fluctuations in eastern Jotunheimen, central southern Norway. The Holocene 18 (8), 1179–1191.
Thompson, L.G., Mosley-Thompson, E., Davis, M.E., et al., 1995. A 1000-year climate ice-record record from the Guliya ice cap, China: its relationship to global climate variability. Ann. Glaciol. 21, 175–181.
Thouveny, N., Carcaillet, J., Moreno, E., et al., 2004. Geomagnetic moment variation and paleomagnetic excursions since 400 kyr BP: a stacked record from sedimentary sequences of the Portuguese margin. Earth Planet. Sci. Lett. 219, 377–396.
van der Bilt, W.G.M., Bakke, J., Vasskog, K., et al., 2015. Reconstruction of glacier activity from lake sediments reveals dynamic of Holocene climate in svalbard. Quat. Sci. Rev.

126, 201–218.
Verosub, K.L., 1977. Depositional and post-depositional processes in the magnetization of sediments. Rev. Geophys. 15 (2), 129–143.
Wang, T., Yang, B., Bräuning, A., et al., 2004. Decadal-scale precipitation variations in arid and semi-arid zones of northern China during the last 500 years. Chin. Sci. Bull. 49 (8), 842–847.
Williams, M.W., Konovalov, V.G., 2008. Central Asia Temperature and Precipitation Data, 1879–2003, Version 1. [Indicate Subset Used]. NSIDC: National Snow and Ice Data Center, Boulder, Colorado USA. https://doi.org/10.7265/N5NK3BZ8.
Wittmeier, H.E., Bakke, J., Vasskog, K., et al., 2015. Reconstructing Holocene glacier activity at Langfjordjøkelen, Arctic Norway, using multi-proxy fingerprinting of distal glacier-fed lake sediments. Quat. Sci. Rev. 114, 78–99.
Yang, B., Bräuning, A., Johnson, K.R., et al., 2002. General characteristics of temperature variation in China during the last two millennia. Geophys. Res. Lett. 29 (9), 1234. https://doi.org/10.1029/2001GL014484.
Yang, B., Wang, J., Bräuning, A., et al., 2009. Late Holocene climatic and environmental changes in arid Central Asia. Quat. Int. 194, 68–78.